COBEM 2021 Florianópolis - Brasil
ABCM Associação Brasileira de Engenharia e Ciências Mecânicas
26th ABCM International Congress of Mechanical Engineering
November 22-26, 2021. Florianópolis, SC, Brazil

COB-2021-0451
ON THE INFLUENCE OF WALL THICKNESS HETEROGENEITY IN THE MECHANICS OF INTRACRANIAL ANEURYSMS

Iago Lessa de Oliveira
José Luiz Gasche
São Paulo State University (UNESP), School of Natural Sciences and Engineering, Ilha Solteira, São Paulo, Brazil
iago.oliveira@unesp.br
jose.gasche@unesp.br

Julio Militzer
Dalhousie University, Department of Mechanical Engineering, Halifax, Nova Scotia, Canada
julio.militzer@dal.ca

Carlos Eduardo Baccin
Interventional Neuroradiology, Hospital Israelita Albert Einstein, São Paulo, Brazil
cebaccin@gmail.com

Philip Cardiff
University College Dublin (UCD), School of Mechanical and Materials Engineering, Dublin, Ireland
philip.cardiff@ucd.ie

Abstract. *Although intracranial aneurysms (IAs) have been extensively investigated in the last three decades by using numerical techniques, the bulk of these works have been focused on using Computational Fluid Dynamics (CFD) to simulate the blood flow, since substantial evidence shows that hemodynamics plays a crucial role in this pathology. However, most works assumed the vascular tissue as rigid, i.e., ignoring the effect of its elasticity. Nevertheless, it is well known that arteries exhibit nonlinear and anisotropic constitutive behavior with heterogeneous mechanical properties. Moreover, the vascular wall does not have uniform thickness. Relatively few works have investigated the impact of wall tissue modeling on the mechanics of IAs: some of them have focused on the hemodynamics without presenting the eventual changes on tissue stress and deformation; while others have numerically simulated the IA sac only — isolating the aneurysm and removing the vascular branches — by using a membrane model approach that assumed a uniform thickness throughout the aneurysm. To have better models to study the mechanics of IAs in a Fluid-Solid Interaction (FSI) context and while patient-specific data is not routinely collected yet, it is important to understand the impact of modeling choices on the wall mechanics of this pathology since an IA rupture, which physicians ultimately try to prevent, is a wall-exclusive event that depends on the level of stresses. In this context, this work investigates the influence of thickness heterogeneity directly on the wall mechanics for the St. Venant-Kirchhoff and the neo-Hookean models by numerically simulating a pressure-inflation model of two patient-specific vasculatures with ruptured and unruptured IAs, collected from medical images. Our results suggest that the uniform thickness modeling choice throughout the vasculature may overestimate or underestimate the von Mises stress on the aneurysm depending on the value of this uniform thickness. Furthermore, this seems to be consistent for different constitutive laws. Therefore, it is essential to account for a realistic modeling of the wall thickness distribution on a vasculature when investigating IA wall mechanics.*
Keywords: *intracranial aneurysms, aneurysm wall mechanics, heterogeneous thickness,* `solids4foam`

1. INTRODUCTION

Intracranial aneurysms (IAs) are pathological dilatations of the human vascular system normally found in the bifurcations of the cerebral arteries tree. This disease has, in the past three decades, been investigated experimentally (Meng *et al.*, 2007; Metaxa *et al.*, 2010), which, for example, led to the understanding of the importance of hemodynamics on its development, but also numerically through Computational Fluid Dynamics (CFD), which provided detailed information on the hemodynamics (Liang *et al.*, 2019) — although still being a debatable topic in the clinical practice (Kallmes, 2012; Cebral and Meng, 2012).

Due to the nature of this pathology, better modeling is continuously sought for more reliable numerical simulations, for example, through the use of Fluid-Solid Interaction (FSI) modeling, which poses challenging numerical difficulties

(Causin *et al.*, 2005; Förster *et al.*, 2007), thus its use is not widespread to simulate blood flow in IAs. Computational Solid Dynamics (CSD) have also been used, for example, to study the IA wall mechanics, with a "forward approach" (Valencia *et al.*, 2013) and the "inverse approach" to determine the stresses on the wall (Ma *et al.*, 2007; Lu *et al.*, 2013). When modeling the aneurysm wall, a further difficulty is the lack of patient-specific data on the wall morphology, such as its thickness, and mechanical properties, such as the tissue's constitutive modeling and its material properties. This is particularly important due to the large variability of the disease.

It is well known that the IAs and their surrounding arteries have different and heterogeneous thicknesses. An earlier study measured the thicknesses of ruptured human IAs and found an average value of 0.51 mm (Abruzzo *et al.*, 1998), and more recent studies have found similar values. Studies performed by Costalat *et al.* (2011) and Robertson *et al.* (2015), for example, found the aneurysm averaged thickness to be around 0.2 to 0.3 mm, and ranging from 0.1 to 0.6 mm. In a similar study, Cebral *et al.* (2015) found an average aneurysm sample thickness of 0.247 mm. On the other hand, according to Robertson *et al.* (2015), intracranial arteries have a larger mean thickness with 0.60 ± 0.12 mm and 0.51 ± 0.08 mm in the basilar and middle cerebral arteries, respectively.

Despite these observations, numerical studies with IA geometries have mostly used uniform wall thicknesses for both arteries and aneurysms (Lee *et al.*, 2013a) and very few directly investigated the influence of a heterogeneous wall thicknesses in different variables. Torii *et al.* (2010), which focused on the hemodynamics, modeled the arteries with an uniform thickness (0.3 mm) and the aneurysm wall with a smaller but also uniform thickness (0.05 mm) — the authors name it a "pathological" wall thickness. They performed FSI simulations and compared the resulting hemodynamics with similar simulations but using a uniform thickness throughout the wall domain (0.3 mm). According to their results, low wall shear stress (WSS) regions appeared to be more pronounced for the pathological wall thickness. However, in their study as well as in others studies, they did not perform any comparison regarding the wall stresses, which would be important because the final rupture of an IA is a wall-exclusive event, whic ultimately occurs when the stress on the wall exceeds the strength of the tissue. Nevertheless, probably because of the focus on the hemodynamics, which is indeed of foremost importance, there is scarce data on the influence of the wall morphology on the tissue stresses. In this context, the aim of this work is to investigate this relation by simulating the motion of IAs walls with heterogeneous thickness under different constitutive models by using pressure-inflation modeling through CSD simulations.

2. NUMERICAL METHODOLOGY

2.1 Mechanical Modeling and Boundary Conditions

Figure 1a shows a schematic two-dimensional drawing of a vascular wall with an IA, the domain Ω^{s}. The tissue material is considered to be materially homogeneous and characterized by its density ρ^{s}, Young's modulus E, and Poisson's ratio ν^{s} — the "s" indicates a "solid" material property. The figure also shows the boundary conditions (BCs). We used two approaches to compute the wall thickness, described in Section 2.2

We modeled the motion of the vasculature wall under conditions similar to inflation experiments where the vessel in subjected to uniform outer and inner pressures — which were already used to study the mechanical properties of IAs (Scott *et al.*, 1972) and also as a modeling approach in numerical simulations (Valencia *et al.*, 2013). The inner surface, which coincides with the vascular lumen, was subjected to a time-varying pressure corresponding to the physiologically normal cardiac cycle, i.e. from 80 to 120 mmHg (approximately 10 to 16 kPa), shown in Fig. 1b. The pressure waveform was derived from a flow profile measured at the internal carotid artery (ICA) of older adults by Hoi *et al.* (2010). Although a full FSI modeling would be more suitable for real IAs geometries, thus taking into account all flow forces on the lumen, this pressure-inflation modeling suffices for the comparative study of different wall mechanics. On the outer (or abluminal) surface, a pressure of $p_o = 5\,\mathrm{mmHg}$, corresponding to the intracranial pressure, was imposed. Although the intracranial pressure seems to vary among patients, we have found similar values in related studies (Valencia *et al.*, 2013; Sanchez *et al.*, 2014).

Regarding the selection of the BC on the branches "sections" (indicated in Fig. 1a), we imposed a fixed zero displacement, which is mathematically written as:

$$\boldsymbol{u} = \boldsymbol{0}\,. \tag{1}$$

There is some controversy on the use of this BC since it is difficult to predict which numerical BC can be realistically applied in these arteries sections. The studies that have simulated CSD or FSI in vascular geometries commonly imposed Eq. (1) too (Lee *et al.*, 2013b; Valencia *et al.*, 2013). However, few works (Bazilevs *et al.*, 2010a) applied a BC that allows the arterial branch to slide along the section's tangential direction, but constrains the displacement along its normal — hence a "zero-shear traction" BC. We performed a numerical study comparing both, and found that, although the displacement field is affected by the different BCs, the stresses remain almost unaltered — mean Von Mises stress difference between each BC less than 2 % —, although the computational performance of the fixed displacement is much better than the zero shear BC, hence we used the former for all simulations.

To solve for the solid displacement, $\boldsymbol{u}$, a finite-strain modeling was assumed, and we used the total Lagrangian (TL)

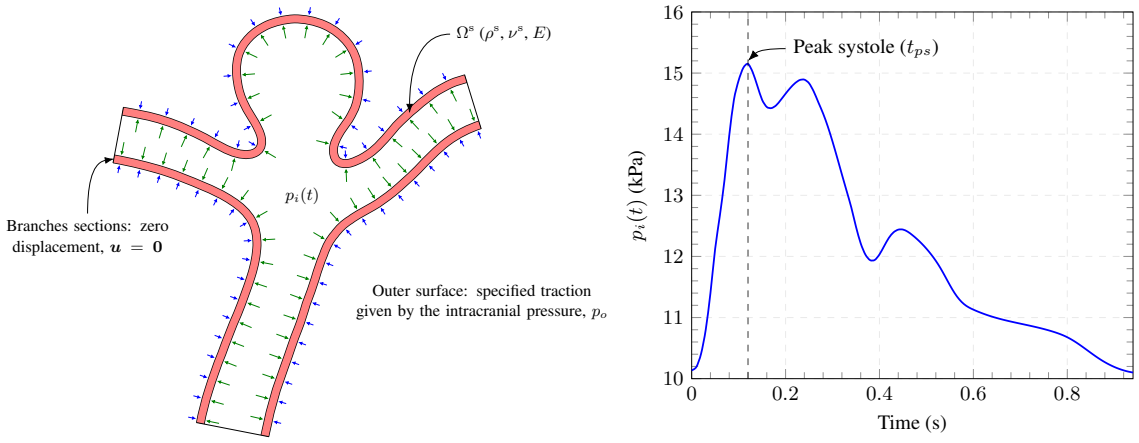

(a) (b)

Figure 1. (a) Schematic 2D drawing of the vascular wall domain, Ω^s, and the BCs applied; (b) the pressure waveform used, which was computed to be between the normal pressure range 80 to 120 mmHg and its waveform proportional to the blood flow rate profile measured at the ICA of older adults by Hoi *et al.* (2010).

formulation of the momentum equation:

$$\rho_0 \frac{\partial^2 \boldsymbol{u}}{\partial t^2} = \nabla_0 \bullet \left(J \boldsymbol{F}^{-1} \bullet \boldsymbol{\sigma} \right) + \rho_0 \boldsymbol{b} \,, \tag{2}$$

where $\boldsymbol{F}$ is the deformation gradient and $J = \det(\boldsymbol{F})$, $\boldsymbol{\sigma}$ is the Cauchy stress tensor, and $\boldsymbol{b}$ represent any body force per unit mass, which were neglected. The subscript "0" indicates any property or derivative taken with respect to the reference configuration, which was considered to be the domain configuration at the time zero and stress-free.

The Cauchy stress tensor in Eq. (2) was assumed to be given by two constitutive models suitable for finite strain — both have been used before to solve for the motion of IAs geometries (Torii *et al.*, 2008; Bazilevs *et al.*, 2010b,a) — to assess whether our results for different thickness were consistent between different material laws. The St. Venant-Kirchhoff (SVK) model, with constitutive equation given by:

$$\boldsymbol{S} = 2\mu^s \boldsymbol{E} + \lambda^s \operatorname{tr}(\boldsymbol{E}) \boldsymbol{I} \,, \tag{3}$$

where $\boldsymbol{S}$ is the second Piola-Kirchhoff stress tensor — related to the Cauchy stress tensor by $\boldsymbol{\sigma} = J^{-1} \boldsymbol{F} \bullet \boldsymbol{S} \bullet \boldsymbol{F}^{\mathrm{T}}$ — and $\boldsymbol{E}$ is the Green-Lagrange strain; μ^s and λ^s are the Lamé's material constants given by:

$$\mu^s = \frac{E}{2(1+\nu^s)} \,, \tag{4}$$

$$\lambda^s = \frac{\nu^s E}{(1+\nu^s)(1-2\nu^s)} \,, \tag{5}$$

for a triaxial stress state. The other model was the compressible neo-Hookean (CNH) model with the following constitutive equation:

$$J\boldsymbol{\sigma} = \frac{\kappa^s}{2} \left(J^2 - 1 \right) \boldsymbol{I} + \mu^s \operatorname{dev} \boldsymbol{B}^* \,, \tag{6}$$

where $\boldsymbol{B}^*$ is the isochoric part of the left Cauchy-Green deformation tensor, $\boldsymbol{B}^* = J^{-2/3} \boldsymbol{B}$. The material bulk modulus, κ^s was calculated by using its linear definition:

$$\kappa^s = \frac{E}{3(1-2\nu^s)} \,. \tag{7}$$

Both constitutive models are based on the same set of mechanical constants: the density $\rho^s = 1200\,\mathrm{kg/m^3}$, Young's modulus $E = 1\,\mathrm{MPa}$, and $\nu^s = 0.45$, typical material constants characteristic of rubbery materials and that already have been used to model arteries and IAs tissue (Bazilevs *et al.*, 2010a).

2.2 Geometries and Computation of the Wall Thickness

We selected two vascular geometries (one of them with only one aneurysm and the other with two aneurysms) obtained from digital subtraction angiography (DSA) examinations collected retrospectively. The DSA images were segmented using the Vascular Modeling Toolkit (VMTK)® library (VMTK, 2017) with the level-sets segmentation approach (Piccinelli *et al.*, 2009). Figure 2 shows the surfaces of each case, labeled as follows: case A, a patient-specific unruptured aneurysm in the ICA bifurcation with a very regular surface, without lobular regions and/or blebs; and case B, a vasculature with a ruptured aneurysm located in the ICA bifurcation and an unruptured one located in the middle cerebral artery (MCA) bifurcation.

We used two different approaches to select the thickness of the selected vascular walls. A uniform thickness throughout the vascular geometry, e_{uw}, chosen to be a value close to the average IAs thickness depending on the parent artery for each case, i.e. ≈ 0.1 to $0.2\,\text{mm}$, as reported by works that experimentally measured the thickness of aneurysm sample strips (Costalat *et al.*, 2011; Robertson *et al.*, 2015).

The other approach was to build a heterogeneous thickness field over the vasculature, S_v — the surface without the aneurysm sac —, based on the so-called wall-to-lumen ratio (WLR), and a uniform thickness, e_a, on the aneurysm sac surface only, S_a. We describe the procedure used to compute this heterogeneous thickness field below and the resulting fields for the two geometries used in this work can also be seen in Fig. 2. The images clearly show that e_a is an intermediate value of the immediate surrounding vasculature's thickness. However, note that they do not coincide with the uniform thickness considered for the whole geometry, e_{uw}, since the latter was inferred from measurements.

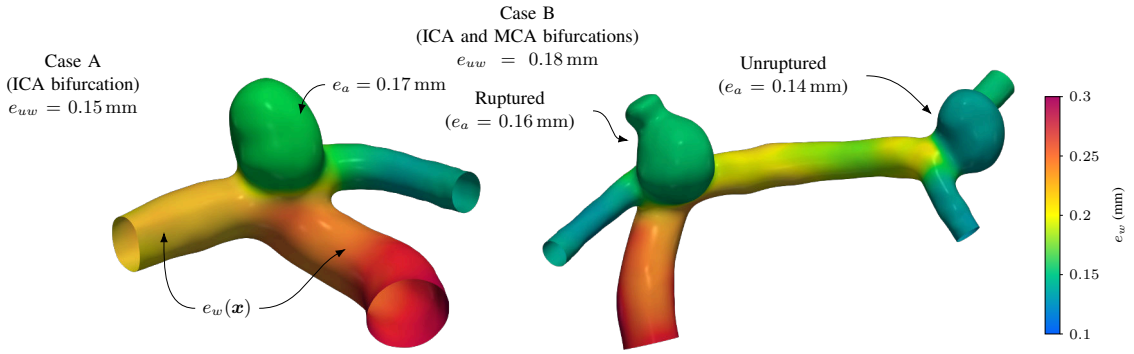

Figure 2. IAs geometries selected with the thickness distribution field of each case and an indication of the whole vasculature thickness distribution, e_w, computed using Eq. (9), and the aneurysm thickness, e_a, computed with Eq. (10). The labels also show the uniform wall thickness, e_{uw}, used for each geometry.

The WLR is defined as:

$$WLR \equiv \frac{\text{artery wall thickness}}{\text{artery lumen diameter}} = \frac{e_w}{d_l}\,, \tag{8}$$

where d_l is the artery lumen diameter at a specified position along the vasculature. Nakagawa *et al.* (2016) reported empirical values of the WLR for the cerebral arteries by measuring it in patients being operated. Their results show that the mean WLR for different medium-sized intracranial arteries (d_l between 2 to 3 mm) is 0.070 ± 0.010 and for large-sized ones ($d_l > 3\,\text{mm}$) is 0.088 ± 0.012.

By using Eq. (8), the thickness of the *vasculature* can be computed as a function of the WLR and the *local* artery lumen diameter, $d_l(\boldsymbol{x})$:

$$e_w\left(\boldsymbol{x}\right) = WLR\, d_l\left(\boldsymbol{x}\right)\,. \tag{9}$$

where d_l was calculated using the script `vmtkdistancetocenterlines` of the VMTK® library, which computes the distance between the vasculature *centerlines* and its surface, as defined by (Piccinelli *et al.*, 2009). This procedure provides a measure of the vasculature's local radius and, consequently, its local diameter. We used WLR $= 0.07$ to keep the consistency among all cases.

This procedure fails to provide the aneurysm thickness because there is no meaningful definition of an "aneurysm's centerline", in this context, or of the aneurysm WLR. In this work, we assumed that the aneurysm thickness is uniform, e_a, and given by an average of the surrounding vasculature thickness field. Thus, based on e_w computed using Eq. (9),

initially ignoring the aneurysm, e_a is calculated by:

$$e_a = f_a \frac{\int_{S_v} l_n\left(\boldsymbol{x}\right) e_w\left(\boldsymbol{x}\right) \mathrm{d}S_v}{\int_{S_v} l_n\left(\boldsymbol{x}\right) \mathrm{d}S_v}\,, \tag{10}$$

where f_a is a factor between 0 and 1 to control how thinner the aneurysm wall is compared to the vasculature — this allowed us to control whether the resulting aneurysm thickness lied between the range of measured IA's thicknesses mentioned in Section 1. A value of 0.75 was used for the geometries chosen for this study. The quantity l_n, serving as a weight function, is the minimum Euclidean distance between each point of the surrounding vasculature's surface, S_v, and the line that separates the aneurysm from the vasculature. Note that this line may not be coincident with the aneurysm *neck line*, because, depending on its morphology and location, there might exist regions that are not originally from the vasculature but, also, are not normally characterized as a portion of the aneurysm sac. Therefore, this line may be imagined as a separation between the *hypothetical healthy vasculature* and the *aneurysm influence region*. We selected this line manually on the vascular geometry. Finally, the separation between the vasculature's thickness field and the aneurysm region was smoothed to avoid discontinuities, which are not biologically realistic.

2.3 Computational Meshes and Numerical Strategies

The triangulated surfaces extracted with VMTK® were re-meshed by using the utility `cartesianMesh` provided by `foam-extend` as part of the `cfMesh` library. This yields a surface mesh with polygonal faces, in general, but dominated by quadrilateral faces. Then, the computational meshes, both with uniform and heterogeneous thickness, were created by extruding the polygonal surfaces in the outward direction with the thicknesses defined in Section 2.2 , e_w, using the VMTK® script `vmtkboundarylayer`, which has support for a spatially-varying thickness field.

The governing equation, Eq. (2), was solved by using a segregated algorithm implemented in `solids4foam` (Cardiff *et al.*, 2018), an extension of the `foam-extend` library (foam-extend Project, 2017; Weller *et al.*, 1998), version 4.0, which uses the second-order accurate Finite Volume Method (FVM) as discretization method. To assure this accuracy level of the spatial discretization, only second-order interpolation profiles were selected: the central differences for the Laplacian terms with non-orthogonal and skewness corrections and the least-squares method for the gradient's discretization (Jasak, 1996). The temporal term was discretized by using the implicit Euler approach.

A mesh-independence study was carried out and yielded a mesh with cells density of approximately 90 cells/mm^2 with 3 cells along the thickness — changes of less the 3 % were found with subsequent refinement. We also performed time-step and residuals tolerance independence tests yielding a time-step of 1×10^{-4} s and a normalized residual tolerance for the momentum equation of 1×10^{-7}. Three cardiac pressure cycles of were simulated, but we only analyzed the third cycle to avoid numerical errors associated with the initial transients.

2.4 Data Analysis

We looked at the Von Mises or equivalent stress, defined as:

$$\sigma_0 = \sqrt{\frac{3}{2}\,\mathrm{dev}\left(\boldsymbol{\sigma}\right) \colon \mathrm{dev}\left(\boldsymbol{\sigma}\right)}\,, \tag{11}$$

where $\mathrm{dev}(\boldsymbol{\sigma})$ is the deviatoric component of the Cauchy stress tensor, $\mathrm{dev}\,\boldsymbol{\sigma} \equiv \boldsymbol{\sigma} - \frac{1}{3}\,\mathrm{tr}\left(\boldsymbol{\sigma}\right)\boldsymbol{I}$, with $\boldsymbol{I}$ is the second-order identity tensor. All the results were taken from the *inner surface* of the wall geometries, or lumen of the vasculature, taken at the peak systole instant, t_{ps} (indicated in Fig. 1b), and the results shown in the reference configuration due to the solution of the TL formulation.

We also computed the time-averaged σ_0 on the vascular surface, defined by:

$$\overline{\sigma_0}\left(\boldsymbol{x}\right) = \frac{1}{T}\int_0^T \sigma_0\left(\boldsymbol{x}, t\right)\mathrm{d}t\,, \tag{12}$$

where T is the period of the cardiac cycle. We then evaluated the descriptive statistics of $\overline{\sigma_0}$ distribution over the aneurysm sac surface, S_a, which was delineated manually, and also on the parent artery of each aneurysm, S_{pa} (the parent artery is the artery that "feeds" the aneurysm), — shown in blue and red, respectively, in Fig. 3.

We also analyzed the *aneurysm pulsatility*, δ_v, defined as:

$$\delta_v = \frac{V_{ps} - V_{ld}}{V_{ld}}\,, \tag{13}$$

where V_{ps} and V_{ld} are the aneurysm sac volume at the peak systole and low diastole, respectively.

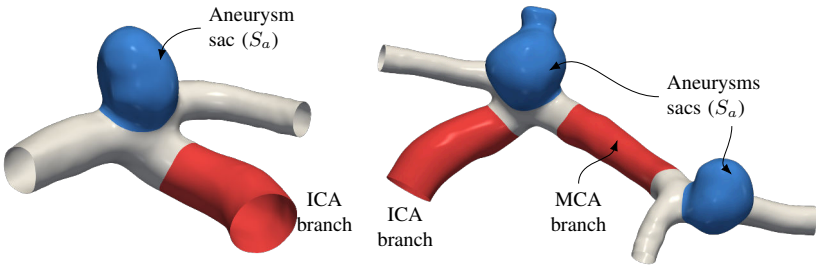

Figure 3. Aneurysm sac surfaces, S_a, marked in blue, and the parent artery surface of each aneurysm, S_{pa}, and to which artery branch it belongs.

3. RESULTS AND DISCUSSIONS

The different wall thickness approaches reveal changes in the stresses on both branches and aneurysms, as can be seen in Fig. 4, which shows the results for the SVK model and also the maximum value of the Von Mises stress, $(\sigma_0)_{max}$ on the aneurysm sac surface annotated next to the aneurysm. This figure suggests a complex relationship between stress and wall thickness. Globally on each geometry and after comparison with Fig. 2, we note that the Von Mises stress seems to increases as the thickness decreases. For example, on the regions where the non-uniform thickness is smaller than the assumed uniform thickness, i.e. $e_w < e_{uw}$, the stress is higher. This occurs in both ruptured and unruptured aneurysms in case B and the opposite in the aneurysm of case A. The same can be found by inspecting the stress on the artery branches. This suggests a similar relationship between stress and thickness that is found for membranes given by the law of Laplace, for example, supported by some studies that mechanically simulated only the aneurysm sac mechanics (Ma *et al.*, 2007; Ramachandran *et al.*, 2012). Finally, we found a similar behavior for the CNH model.

To further investigate this relationship, we looked on the σ_0 distribution in the aneurysms and their parent artery. As can be seen in Fig. 2, although the non-uniform wall thickness applies to the whole *vasculature geometry*, we assumed a uniform thickness throughout the aneurysm sac. The statistics of $\overline{\sigma_0}$ over S_a give a rough indication of the overall level of stress on the aneurysm, allowing a per-aneurysm comparison and, consequently, a per-thickness comparison, as shown in the box plot of Fig. 5, which shows the statistics of the distribution of $\overline{\sigma_0}$ in each aneurysm and also the aneurysm thickness, e_a, along the abscissas axis. It is clear that the $\overline{\sigma_0}$ decreases as e_a increases, although the difference is small and is even less visually perceptible between the ruptured and unruptured aneurysms of case B. However, it is important to note that the ruptured aneurysm of case B have a large lobular region, probably associated with the rupture point of this aneurysm, which distorts the Von Mises stress field distribution due to its curvature, compared to the more regular distribution on the unruptured aneurysms. Thus, it is fairer to compare only the unruptured aneurysm of geometry B with the aneurysm of geometry A.

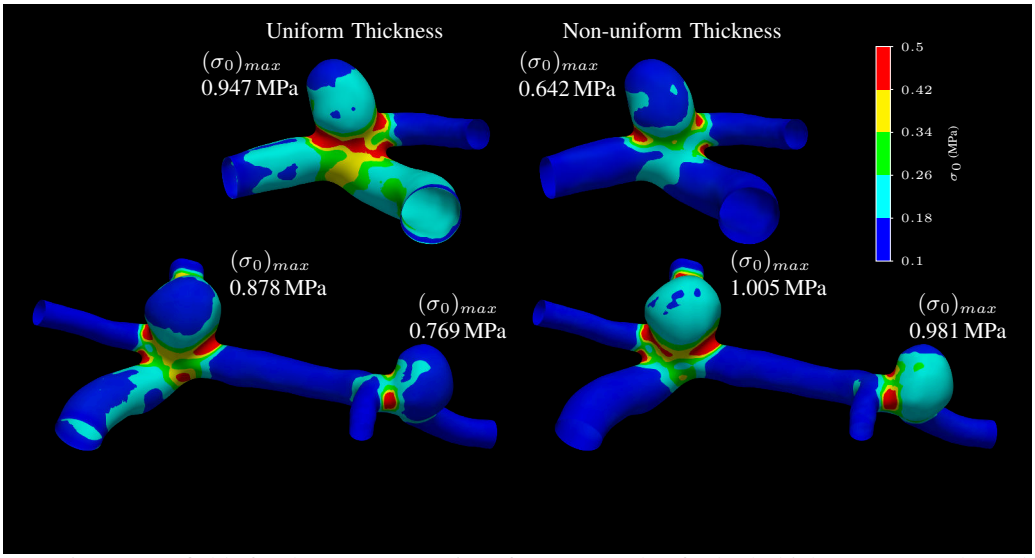

Figure 4. Von Mises stress fields for the IAs geometries of cases B and A for both thickness approaches taken at peak systole (data from the lumen surface and considering the SVK model).

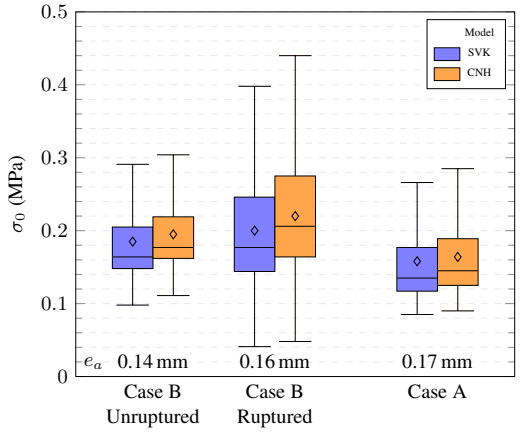

Figure 5. Statistics of the time-averaged Von Mises stress over the aneurysm sac surface, S_a, with an indication of the aneurysm thickness for the different material laws used. Each box marks the interquartile range with the middle line indicating the median and the diamond shape indicates the mean of each distribution.

On the other hand, the branches of the vasculatures effectively have a heterogeneous thickness distribution. Thus, we investigated the correlation between the thickness field, e_w, and $\overline{\sigma_0}$ on the parent artery surface, S_{pa}, of each aneurysm (Fig. 3), after looking at each cell on the surface mesh as a sample datum. We used the Spearman's correlation coefficient, ρ_{S}, to assess the correlation after verifying that the datasets are not normally distributed. The correlation coefficients are shown in Table 1 for each parent artery and for the two material laws. For each correlation, we did not test for significance because the large number of cells on the sample could lead to unrealistically small p-values.

The coefficient ρ_{S} varies between -1 and 1 and values closer to one indicate a strong correlation between the variables. Although the absolute values in Table 1 are smaller than 1, the negative sign indicates that thickness and $\overline{\sigma_0}$ are indeed negatively correlated even for these thick-wall geometries. The strength of the correlation may be small because the relation between the two datasets cannot be fit to a monotonic model.

Table 1. Spearman's correlation coefficient, ρ_{S}, between peak-systole Von Mises stress on the parent artery of each aneurysm, S_{pa}, and the thickness distribution there for the non-uniform wall thickness geometries.

	ρ_{S}	
Model	SVK	CNH
Case A ICA	–0.14	–0.22
Case B MCA	–0.04	–0.13
Case B ICA	0.01	–0.16

The thickness heterogeneity and its influence on the wall stresses was studied by Voß *et al.* (2016) where the authors measured the complete wall thickness distribution by μCT (micro-computed tomography) exams after aneurysm removal of a human cadaver — the patient died of subarachnoid hemorrhage (SAH) caused by an anterior communicating artery (ACoA) aneurysm rupture. Furthermore, after dissection, the rupture point was visible in the aneurysm surface. Therefore, their study focused primarily in the comparison of the structural variables at the rupture point and on the complete aneurysm surface for patient-specific and uniform wall thickness. They found that, for this case specifically, the averaged wall stress on the complete aneurysm surface does not show too much difference although its distribution in significantly changed between the uniform and patient-specific wall thickness. Moreover, in the rupture site specifically, the wall stress difference reaches up to 55.2 %, with the wall stress being much higher at the rupture for the patient-specific thickness. Although we did not investigated the rupture point of the aneurysm of case B, we can see in Fig. 4 that the stresses with the heterogeneous wall thickness is also higher. However, this comparison must be made with caution because we considered the aneurysm wall to be uniform.

Turning our attention to the effect of different material laws used, Fig. 5 already suggests that the CNH seems to overestimate the averaged stresses on the aneurysm sac compared to the SVK model. A qualitative comparison for the whole vascular geometry is shown in Fig. 6 for the non-uniform wall thickness. The figure shows that the CNH model overestimates the Von Mises stress throughout the vasculature and not only on the aneurysm surface, where the percentual difference for $(\sigma_0)_{max}$ is at least 14.4 % among the three aneurysms.

Table 2, which shows the aneurysm pulsatility for the different modeling alternatives, shows that the impact of the change in material law can be as high as 3 times between the SVK and CNH models and the same for different thickness

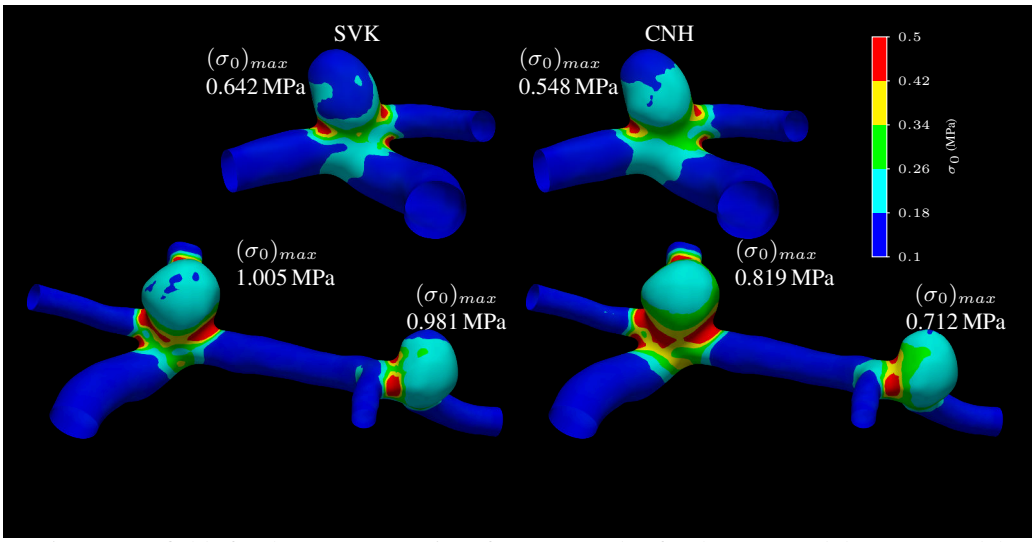

Figure 6. Von Mises stress fields for the IAs geometries of cases A and B for the SVK and the CNH models taken at peak systole (data from the lumen surface and considering the non-uniform wall thickness distribution).

approaches, with the CNH model consistently yielding a larger δ_v, although we cannot infer from the data on the table any consistent changes between different thickness approach. This suggests that the choice of material model and thickness for the aneurysm and artery wall is a very sensible one and cannot be undermined, specially when predicting parameters that may have a clinical relevance, such as δ_v.

Table 2. IA pulsatility, δ_v, for each geometry and for different material law and thickness approach used (values given in percent).

Modeling		Non-uniform		Uniform	
		SVK	CNH	SVK	CNH
Case A		9.8	22.2	11.3	42.4
Case B	Ruptured	12.2	44.9	11.0	32.1
	Unruptured	11.2	30.5	9.2	19.1

We found few studies that directly assessed the influence of material law modeling choices on the mechanics of patient-specific IAs. Torii *et al.* (2008), for example, ran FSI simulations with the rigid wall assumption, the Hookean solid, the SVK solid, and an exponential hyperelastic model proposed by Demiray (1972) — they used a uniform wall thickness for the whole geometry of 0.3 mm. Their findings show that the displacement profiles were qualitatively similar for all models, although the maximum displacement for the hyperelastic model is 36 % smaller than that for the SVK, against our results that indicates much larger displacements yielded by the CNH, which is also a hyperelastic model, but different from the one they used. Nevertheless, it is also reasonable to speculate that the pressure-inflation modeling may overestimate both displacements and stresses compared to an FSI simulation due to the smaller pressures that may occur in the flow that are used to simulate the solid wall. Additionally, the authors did not present any data on the wall stresses, hence not allowing us to draw any further comparison with our data.

On the other hand, Ramachandran *et al.* (2012) investigated the impact of different constitutive models on the wall stresses and strains specifically by numerically simulating the aneurysm sac with an "inverse approach" strategy that only accounts for the aneurysm wall and using a static pressure-inflation model, similar to the model used here. They employed both anisotropic and isotropic versions of a Fung-like model, the Yeoh model with three parameters, the SVK, and the Hookean models. Their results suggest that different modeling choices had little impact on wall tensions and that Laplace's law was the worst method to estimate the stress, suggesting a deviation from the membrane model. Furthermore, the authors highlight that these conclusions may not withstand when the full vasculature is simulated with dynamical BCs that realistically reflect the cardiac cycle forces. This is inline with our current study, since we verified substantial changes according to the material law used, not only on stresses but also on the pulsatility index, independently of the thickness approach used, even though we have used a simplified pressure-inflation model.

4. CONCLUSIONS

In recent years, an increasingly amount of studies have simulated the wall mechanics of IAs through the use of FSI and CSD. However, the lack of patient-specific data on the wall morphology and tissue properties renders a precise modeling very challenging. In this context, our study helps to understand the influence of simplifying assumptions on the results of numerical simulations, particularly on the stress in the aneurysm wall, which is relevant to better judge the results of FSI simulations, for example.

We found that the stresses are influenced by the heterogeneous thickness distribution of the aneurysm and its surrounding branches, hence it is better to avoid the use of uniform thickness when simulating IA wall motion. It seems that the stresses, in this case represented by the equivalent or Von Mises stress, decreases as the thickness increases, and this result was enforced by an analysis on both the aneurysm sac and on the branches of the vasculatures used. Furthermore, this behavior was consistent between two different constitutive models, the SVK and the CNH models, with the CNH model overestimating the stresses in the overall vascular wall.

A next step in this research is to incorporate the aneurysm thickness heterogeneity, which was already obtained in experimental studies using 7T Magnetic Resonance Imaging (MRI) (Kleinloog *et al.*, 2014). However, the technique is not already common and have not been validated in clinical practice, hence it is still a challenge to obtain the thickness of a patient-specific vasculature. The aneurysm thickness distribution may be fairly complex and not necessarily close to the surrounding vasculature thickness, on the contrary, there may be cases where the aneurysm is thicker than its parent vasculature, for example, when it presents atherosclerotic regions (Meng *et al.*, 2014; Voß *et al.*, 2016). Incorporating this heterogeneity would be essential for better modeling of the aneurysm wall motion and are already under study by our group, which could further enhance the understanding of this dangerous disease.

5. ACKNOWLEDGEMENTS

This research is supported by grant 2017/18514-1 and 2019/19098-7 of São Paulo Research Foundation (FAPESP). It was also supported by resources supplied by the Center for Scientific Computing (NCC/GridUNESP) of the São Paulo State University (UNESP) (`www2.unesp.br/portal#!/gridunesp`), by ACENET (`www.ace-net.ca`) through Dalhousie University and Compute Canada (`www.computecanada.ca`).

6. REFERENCES

Abruzzo, T., Shengelaia, G.G., Dawson, R.C., Owens, D.S., Cawley, C.M. and Gravanis, M.B., 1998. "Histologic and Morphologic Comparison of Experimental Aneurysms with Human Intracranial Aneurysms". *American Journal of Neuroradiology*, Vol. 19, pp. 1309–1314.

Bazilevs, Y., Hsu, M.C., Zhang, Y., Wang, W., Kvamsdal, T., Hentschel, S. and Isaksen, J.G., 2010a. "Computational vascular fluid-structure interaction: Methodology and application to cerebral aneurysms". *Biomechanics and Modeling in Mechanobiology*, Vol. 9, pp. 481–498. ISSN 16177959. doi:10.1007/s10237-010-0189-7.

Bazilevs, Y., Hsu, M.C., Zhang, Y., Wang, W., Liang, X., Kvamsdal, T., Brekken, R. and Isaksen, J.G., 2010b. "A fully-coupled fluid-structure interaction simulation of cerebral aneurysms". *Computational Mechanics*, Vol. 46, pp. 3–16. ISSN 01787675. doi:10.1007/s00466-009-0421-4.

Cardiff, P., Karač, A., De Jaeger, P., Jasak, H., Nagy, J., Ivanković, A. and Tuković, Ž., 2018. "An open-source finite volume toolbox for solid mechanics and fluid-solid interaction simulations". Technical report.

Causin, P., Gerbeau, J.F. and Nobile, F., 2005. *Added-Mass Effect in the Design of Partitioned Algorithms for Fluid-Structure Problems*. Ph.D. thesis. doi:10.1016/j.cma.2004.12.005.

Cebral, J.R., Duan, X., Chung, B.J., Putman, C., Aziz, K. and Robertson, A.M., 2015. "Wall mechanical properties and hemodynamics of unruptured intracranial aneurysms". *American Journal of Neuroradiology*, Vol. 36, No. 9, pp. 1695–1703. ISSN 1936959X. doi:10.3174/ajnr.A4358.

Cebral, J.R. and Meng, H., 2012. "Counterpoint: Realizing the Clinical Utility of Computational Fluid Dynamics—Closing the Gap". doi:10.3174/ajnr.a2993.

Costalat, V., Sanchez, M., Ambard, D., Thines, L., Lonjon, N., Nicoud, F., Brunel, H., Lejeune, J.P., Dufour, H., Bouillot, P., Lhaldky, J.P., Kouri, K., Segnarbieux, F., Maurage, C.A., Lobotesis, K., Villa-Uriol, M.C., Zhang, C., Frangi, A.F., Mercier, G., Bonafé, A., Sarry, L. and Jourdan, F., 2011. "Biomechanical wall properties of human intracranial aneurysms resected following surgical clipping (IRRAs Project)". *Journal of Biomechanics*, Vol. 44, No. 15, pp. 2685–2691. doi:10.1016/j.jbiomech.2011.07.026.

Demiray, H., 1972. "A note on the elasticity of soft biological tissues". *Journal of Biomechanics*, Vol. 5, pp. 309–311. doi:10.1016/0021-9290(72)90047-4.

foam-extend Project, 2017. "foam-extend Website". `https://sourceforge.net/projects/foam-extend/`. [Accessed 19-June-2017].

Förster, C., Wall, W.A. and Ramm, E., 2007. "Artificial added mass instabilities in sequential staggered coupling of

nonlinear structures and incompressible viscous flows". *Computer Methods in Applied Mechanics and Engineering*, Vol. 196, No. 7, pp. 1278–1293. ISSN 00457825. doi:10.1016/j.cma.2006.09.002.

Hoi, Y., Wasserman, B.A., Xie, Y.J., Najjar, S.S., Ferruci, L., Lakatta, E.G., Gerstenblith, G. and Steinman, D.A., 2010. "Characterization of volumetric flow rate waveforms at the carotid bifurcations of older adults". *Physiological Measurement*, Vol. 31, No. 3, pp. 291–302. ISSN 09673334. doi:10.1088/0967-3334/31/3/002.

Jasak, H., 1996. *Error Analysis and Estimation for the Finite Volume Method with Applications to Fluid Flows*. Ph.D. thesis, Imperial College.

Kallmes, D.F., 2012. "Point: CFD—Computational Fluid Dynamics or Confounding Factor Dissemination". *American Journal of Neuroradiology*, Vol. 33, pp. 393–398. doi:10.3174/ajnr.A2993.

Kleinloog, R., Korkmaz, E., Zwanenburg, J.J.M., Kuijf, H.J., Visser, F., Blankena, R., Post, J.A., Ruigrok, Y.M., Luijten, P.R., Regli, L., Rinkel, G.J.E. and Verweij, B.H., 2014. "Visualization of the aneurysm wall: A 7.0-tesla magnetic resonance imaging study". *Neurosurgery*, Vol. 75, No. December, pp. 614–622. doi:10.1227/NEU.0000000000000559.

Lee, C.J., Zhang, Y., Takao, H., Murayama, Y. and Qian, Y., 2013a. "A fluid-structure interaction study using patient-specific ruptured and unruptured aneurysm: The effect of aneurysm morphology, hypertension and elasticity". *Journal of Biomechanics*, Vol. 46, No. 14, pp. 2402–2410. ISSN 00219290. doi:10.1016/j.jbiomech.2013.07.016.

Lee, C.J., Zhang, Y., Takao, H., Murayama, Y. and Qian, Y., 2013b. "The influence of elastic upstream artery length on fluid-structure interaction modeling: A comparative study using patient-specific cerebral aneurysm". *Medical Engineering and Physics*, Vol. 35, No. 9, pp. 1377–1384. ISSN 13504533. doi:10.1016/j.medengphy.2013.03.009.

Liang, L., Steinman, D.A., Brina, O., Chnafa, C., Cancelliere, N.M. and Pereira, V.M., 2019. "Towards the Clinical utility of CFD for assessment of intracranial aneurysm rupture - A systematic review and novel parameter-ranking tool". *Journal of NeuroInterventional Surgery*, Vol. 11, pp. 153–158. ISSN 17598486. doi:10.1136/neurintsurg-2018-014246.

Lu, J., Hu, S. and Raghavan, M.L., 2013. "A Shell-Based Inverse Approach of Stress Analysis in Intracranial Aneurysms". *Annals of Biomedical Engineering*, Vol. 41, No. 7, pp. 1505–1515. ISSN 0090-6964, 1573-9686. doi:10.1007/s10439-013-0751-4.

Ma, B., Lu, J., Harbaugh, R.E. and Raghavan, M.L., 2007. "Nonlinear Anisotropic Stress Analysis of Anatomically Realistic Cerebral Aneurysms". *Journal of Biomechanical Engineering*, Vol. 129, No. 1, pp. 88–96. ISSN 0148-0731, 1528-8951. doi:10.1115/1.2401187.

Meng, H., Tutino, V.M., Xiang, J. and Siddiqui, A., 2014. "High WSS or Low WSS? Complex interactions of hemodynamics with intracranial aneurysm initiation, growth, and rupture: Toward a unifying hypothesis". *American Journal of Neuroradiology*, Vol. 35, No. 7, pp. 1254–1262. ISSN 1936959X. doi:10.3174/ajnr.A3558.

Meng, H., Wang, Z., Hoi, Y., Gao, L., Metaxa, E., Swartz, D.D., Kolega, J., Swartz, D.D. and Kolega, J., 2007. "Complex Hemodynamics at the Apex of an Arterial Bifurcation Induces Vascular Remodeling Resembling Cerebral Aneurysm Initiation". *Stroke*, Vol. 38, pp. 1924–1931. doi:10.1161/STROKEAHA.106.481234.

Metaxa, E., Tremmel, M., Natarajan, S.K., Xiang, J., Paluch, R.A., Mandelbaum, M., Siddiqui, A.H., Kolega, J., Mocco, J. and Meng, H., 2010. "Characterization of critical hemodynamics contributing to aneurysmal remodeling at the basilar terminus in a rabbit model". *Stroke*, Vol. 41, No. 8, pp. 1774–1782. ISSN 00392499. doi:10.1161/STROKEAHA.110.585992.

Nakagawa, D., Shojima, M., Yoshino, M., Kin, T., Imai, H., Nomura, S., Saito1, T., Nakatomi, H., Oyama1, H. and Saito, N., 2016. "Wall-to-lumen ratio of intracranial arteries measured by indocyanine green angiography". *Asian Journal of Neurosurgery*, Vol. 11, pp. 361–364. doi:10.4103/1793-5482.175637.

Piccinelli, M., Veneziani, A., Steinman, D.A., Remuzzi, A. and Antiga, L., 2009. "A framework for geometric analysis of vascular structures: Application to cerebral aneurysms". *IEEE Transactions on Medical Imaging*, Vol. 28, No. 8, pp. 1141–1155. doi:10.1109/TMI.2009.2021652.

Ramachandran, M., Laakso, A., Harbaugh, R.E. and Raghavan, M.L., 2012. "On the role of modeling choices in estimation of cerebral aneurysm wall tension". *Journal of Biomechanics*, Vol. 45, No. 16, pp. 2914–2919. ISSN 00219290. doi:10.1016/j.jbiomech.2012.07.029.

Robertson, A.M., Duan, X., Aziz, K.M., Hill, M.R., Watkins, S.C. and Cebral, J.R., 2015. "Diversity in the Strength and Structure of Unruptured Cerebral Aneurysms". *Annals of Biomedical Engineering*, Vol. 43, No. 7, pp. 1502–1515. doi:10.1007/s10439-015-1252-4.

Sanchez, M., Ecker, O., Ambard, D., Jourdan, F., Nicoud, F., Mendez, S., Lejeune, J.P., Thines, L., Dufour, H., Brunel, H., Machi, P., Lobotesis, K., Bonafe, A. and Costalat, V., 2014. "Intracranial aneurysmal pulsatility as a new individual criterion for rupture risk evaluation: Biomechanical and numeric approach (IRRAs Project)". *American Journal of Neuroradiology*, Vol. 35, pp. 1765–1771. doi:10.3174/ajnr.A3949.

Scott, S., Ferguson, G.G. and Roach, M.R., 1972. "Comparison of the Elastic Properties of Human Intracranial Arteries and Aneurysms". *Canadian Journal of Physiology and Pharmacology*, Vol. 50, No. 4, pp. 328–332. ISSN 0008-4212. doi:10.1139/y72-049.

Torii, R., Oshima, M., Kobayashi, T., Takagi, K. and Tezduyar, T.E., 2008. "Fluid-structure interaction modeling of a

patient-specific cerebral aneurysm: Influence of structural modeling". *Computational Mechanics*, Vol. 43, pp. 151–159. ISSN 01787675. doi:10.1007/s00466-008-0325-8.

Torii, R., Oshima, M., Kobayashi, T., Takagi, K. and Tezduyar, T.E., 2010. "Influence of wall thickness on fluid–structure interaction computations of cerebral aneurysms". *International Journal for Numerical Methods in Biomedical Engineering*, Vol. 26, pp. 336–347. ISSN 20407939. doi:10.1002/cnm.

Valencia, A., Burdiles, P., Ignat, M., Mura, J., Bravo, E., Rivera, R. and Sordo, J., 2013. "Fluid structural analysis of human cerebral aneurysm using their own wall mechanical properties". *Computational and Mathematical Methods in Medicine*, Vol. 2013, pp. 1–18. ISSN 1748670X. doi:10.1155/2013/293128.

VMTK, 2017. "VMTK Website". `http://www.vmtk.org/`. [Accessed 19-June-2017].

Voß, S., Glaßer, S., Hoffmann, T., Beuing, O., Weigand, S., Jachau, K., Preim, B., Thévenin, D., Janiga, G. and Berg, P., 2016. "Fluid-Structure Simulations of a Ruptured Intracranial Aneurysm: Constant versus Patient-Specific Wall Thickness". *Computational and Mathematical Methods in Medicine*, Vol. 2016. doi:10.1155/2016/9854539.

Weller, H.G., Tabor, G., Jasak, H. and Fureby, C., 1998. "A tensorial approach to computational continuum mechanics using object-oriented techniques". *Computers in Physics*, Vol. 12, pp. 620–631.

7. RESPONSIBILITY NOTICE

The authors are solely responsible for the printed material included in this paper.